Chemical Engineering Journal 461 (2023) 141904

Contents lists available at ScienceDirect

Chemical Engineering Journal

journal homepage: www.elsevier.com/locate/cej

A localized high concentration carboxylic ester-based electrolyte for high-voltage and low temperature lithium batteries

Pengbin Lai [a], Boyang Huang [a], Xiaodie Deng [a], Jialin Li [a], Haiming Hua [a], Peng Zhang [b,*], Jinbao Zhao [a,b,*]

[a] State-Province Joint Engineering Laboratory of Power Source Technology for New Energy Vehicle, Engineering Research Center of Electrochemical Technology, Ministry of Education, College of Chemistry and Chemical Engineering, Xiamen University, Xiamen 361005, PR China
[b] College of Energy, Xiamen University, Xiamen 361102, PR China

ARTICLE INFO

Keywords:
Localized high concentration electrolyte
Methyl propionate
High voltage
Fast dynamic
Low temperature

ABSTRACT

In this work, a methyl propionate (MP)/fluoroethylene carbonate (FEC)-based localized high concentration electrolyte with lithium difluoro(oxalato)borate (LiDFOB) as the additive is reported. The tuned solvation structure and the addition of LiDFOB enable fast desolvation process of Li^+ and good formation of cathode/electrolyte interphase. This optimized electrolyte shows good compatibility with both lithium cobaltate (LCO) cathode and lithium metal anode, enabling 4.5 V Li/LCO cell to cycle 300 cycles at 1C (180 mAh g^{-1}) rate with 87.7 % capacity retention. Even at 10C high-rate cycling, around 75.0 % of initial capacity is also achieved. In addition, it possesses decent conductivity and viscosity at low temperature, demonstrating the great low-temperature performance. It enables the high-loading Li/LCO cell to deliver 136.9 mAh g^{-1}capacity at −70 °C, showing the great discharge performance and application potential at such low temperature. In addition, the cell with this electrolyte could even be cycled at −40 °C with 77.8 % capacity retention after 100 cycles. This work implements the high-voltage, high-rate and low-temperature functions of battery by choosing appropriate electrolyte component and tuning its formulation. This work provides an effective method for designing a multifunctional lithium battery electrolyte.

1. Introduction

Lithium ion batteries (LIBs) [1–4] have been extensively applied in every aspect of our life since the commercialization in the early 1990 s. However, traditional LIBs could not meet the ever-growing demand for higher energy density [5]. What is worse, when the temperature was decreased below sub-zero, traditional LIBs deliver much lower capacity than that at room temperature, restricting its application in extremely cold field like electric vehicles, expedition, aerospace etc. [6–10] Therefore, developing the high-energy–density battery with wide-temperature adaptability is of great emergence.

The effective way to satisfy these demands above is to use the high-voltage cathode paired with lithium metal anode (LMA). The LMA is a promising anode because it not only has high theoretical capacity (3860 mAh g^{-1}) and low reductive potential (-3.04 V vs Standard Hydrogen Electrode), but also has better kinetic than traditional graphite's intercalation chemistry at low temperature [11–14]. As for the high-voltage cathode, lithium cobaltate (LCO) is a competitive candidate for its high theoretical capacity, high working voltage and fast lithium-ion diffusion within the crystal lattice even at low temperature condition [15]. Unfortunately, the application of cell contained the high-voltage LCO and lithium metal is limited because there is a lack of appropriate electrolyte to match with. The commonly-used carbonate electrolyte is easily oxidized and decomposed at high voltage for its low oxidation potential (≈ 4.3 V vs Li/Li^+) [16,17]. On the other hand, the carbonate electrolyte tends to react with lithium metal, leading to the continuous consumption of electrolyte and degradation of cycling performance [18]. In addition, the melting point of carbonate solvent is relatively high and its binding ability with Li^+ is very strong, which restrict its application in low temperature condition [9,19]. Therefore, it is very crucial to design a new type of electrolyte to guarantee these cells to work stably in wide temperature range.

An ideal electrolyte for the high-voltage and low-temperature cell should meet the following requirements [7,8]: (1) the chemical and

* Corresponding authors at: State-Province Joint Engineering Laboratory of Power Source Technology for New Energy Vehicle, Engineering Research Center of Electrochemical Technology, Ministry of Education, College of Chemistry and Chemical Engineering, Xiamen University, Xiamen 361005, PR China (J. Zhao).
E-mail addresses: pengzhang@xmu.edu.cn (P. Zhang), jbzhao@xmu.edu.cn (J. Zhao).

https://doi.org/10.1016/j.cej.2023.141904
Received 29 November 2022; Received in revised form 16 January 2023; Accepted 12 February 2023
Available online 14 February 2023

electrochemical stability with two electrodes at both cathodic and anodic side to realize a high working voltage; (2) keeping in the liquid state with decent conductivity and viscosity at low temperature to promote efficient ionic conduction; (3) the ability ensuring both the high reversibility of insertion-extraction process of LCO and dissolution-deposition mechanism of lithium metal anode thus to have a chance to gain a stable cycle performance; (4) fast desolvation process during cycling, which is the determined kinetic step for the whole electrochemical process especially at low temperature. The strategies of high voltage and low temperature electrolyte include using film-forming additives [20–22], applying fluorine solvents [23,24], increasing the concentration of salt to form the high concentration electrolyte (HCE) or introducing diluent to HCE system to form the localized high concentration electrolyte (LHCE) [25,26] and so on. Among them, LHCE is a promising method to meet all of the requirements above. The LHCE not only possesses the anion-rich solvation structure as HCE does, but also demonstrated lower viscosity than HCE. And it is worth noting that when the temperature was further decreased, the conductivity of LHCE may surpass the HCE [27]. Feng et al. [28] designed lithium tetrafluoroborate ($LiBF_4$) in FEC / MA / 1,1,2,2-tetrafluoroethyl methyl ether (TFME) electrolyte, realizing the 4.9 V high voltage Li/LNMO cell to work at −50 °C. Besides, the low temperature cycling performance of LHCE can be optimized by the proper selection of component as solvent and lithium salt. In the work of Holoubek et al. [29], the 1 M lithium bis (fluorosulfonyl)imide (LiFSI) in bis (2,2,2 trifluoro ethyl) ether (BTFE) / 1,2-dimethoxyethane (DME) (5: 1) LHCE is developed, which enabled 4.4 V Li/NCM811 full cell to cycle stably at −40 °C with the rate of 0.1C. Also, our previous work [30] reported a 2 m dual-salt sulfone / ethyl acetate-based LHCE that enabled 4.6 V Li/NCM523 cell to cycle at low temperature and remained around 65 % capacity at 10C rate, indicating the advantage of LHCE at high rate performance. All of these works reveal the application potential of LHCE in the field of high voltage, high rate and low temperature. While their application in the ultra-low temperature field (-70 °C) has been seldom explored and researched. Therefore, the formula of LHCE should be precisely selected and compared.

In this work, the carboxylic ester solvent is selected as the main solvent. Comparing with carbonate electrolyte, this kind of solvents has the low melting point, better salt solubility and the most important, the lower binding energy with Li^+, which is very crucial for the improvement of cell's low temperature performance. (Table 1) Among this kind of solvents, methyl propionate (MP) has been widely used as the solvent or co-solvent of low temperature electrolyte in previous literature for its better electrochemical performance in LIBs [31–35]. However, its application in lithium metal batteries (LMBs) is restricted for its higher reactivity with lithium metal anode. What's worse, once the working voltage is higher than 4.2 V, MP solvent also suffer from oxidation reaction at the cathode side. Therefore, just using carboxylic ester co-solvent is not enough to enable the LMBs to work at high voltage.

Table 1
The physical property and binding energy with Li^+ of different solvents.

Solvent	Melting point (°C)	Boiling point (°C)	Dielectric constant	Binding energy (eV)
Ethylene carbonate (EC)	39	248	89.6 (40 °C)	−2.26
Fluorinated Ethylene carbonate (FEC)	18	212	100.3	−2.03
Propylene carbonate (PC)	−49.2	241	64.4	−2.33
Dimethyl carbonate (DMC)	3	90	3.1	−2.00
Diethyl carbonate (DEC)	−43	127	2.8	−2.13
Methyl Formate (MF)	−99	32	8.5	−1.92
Ethyl Acetate (EA)	−83	77	6	−2.16
Methyl Propionate (MP)	−88	80	6.2	−2.13
Methyl Butyrate (MB)	−84	103	5.5	−2.16

To solve these obstacles, we firstly mix the MP and FEC solvent. FEC is proved as an effective component to inhibit the side reaction with lithium metal anode but too much FEC is detrimental to the cell's low temperature performance due to its relatively high melting point [36]. Therefore, MP and FEC were mixed by the volume ratio of 9: 1. And then the LHCE strategy is applied, in which lithium bistrifluoromethanesulfonimide (LiTFSI) is chosen as lithium salt for its higher conductivity and better solubility and 1,1,2,2-tetrafluoroethyl-2,2,2-trifluoroethyl ether (HFE) is selected as a diluent. With the increase of salt concentration, the solvation structure of lithium ion changed from solvent-dominated to anion-dominated, which could stabilize the electrodes at higher voltage and promoted the desolvation process especially at low temperature. Also, the introduction of the diluent reduces the resistance of ion transportation especially at low temperature without changing the solvation structure of HCE. Therefore, the combination of the two strategies is viable and effective in the application scenarios of extreme temperature and high energy density. To further improve the electrochemical performance, little amount of film-forming additive LiDFOB is added into the LHCE, [37,38] forming the optimized electrolyte (OE). The solvation structure and the interfacial chemistry at cathode/electrolyte interface of OE is displayed in Fig. 1a.

With the well-designed electrolyte, the Li/LCO cell maintained 87.7 % capacity after 300 cycles at 1C at room temperature. Apart from that, this electrolyte enables the high-loading cell to deliver 136.9 mAh g^{-1}capacity at −70 °C and to cycle at −40 °C with 77.8 % capacity retention after 100 cycles, demonstrating great low temperature performance. All in all, this work realizes the multi-function of high-voltage, high-rate and low-temperature performance by tuning the solvation structure and adding proper additive, providing an effective method for the design of the multi-functional electrolyte.

2. Experimental section

2.1. Preparation of Materials experimental section

Lithium cobaltate (LCO) active material (>99.5 %) was provided by Beijing Easpring Material Technology Co., ltd. The cathode was prepared by mixing and grinding the cathode active material, acetylene black conductive agent and polyvinylidene fluoride (PVDF) binder by the mass ratio of 8: 1: 1. And then adding the *N*-methyl-2-pyrrolidone (NMP, >99.7 %, Sinopharm Group Co., ltd.) into the mixture to disperse. The formed slurry was magnetically stirred for at least 6 h. As for the high-loading cathode electrode, the mass ratio of the material was 94.5 %: 2.5 %: 3.0 % instead. The stirred slurry was coated on Al foil with the doctor blade and then dried at 80 °C in vacuum oven for 12 h. The mass loading of cathode was around 3 mg cm^{-2} and the high-loading cathode was around 12 mg cm^{-2}. The lithium metal foils (>99.9 %) were purchased from China Energy Lithium Co., ltd, whose diameter were 12 mm and thickness were 200 μm. The separator was purchased from Asahi Kasei Company and its thickness was 20 μm.

The LiTFSI salt, lithium hexafluorophosphate ($LiPF_6$) salt, LiDFOB salt, ethylene carbonate (EC) solvent, dimethyl carbonate (DMC) solvent, HFE diluent (>99 %) were all provided by Zhangjiagang Guotai Huarong New Chemical Materials Co., ltd and their purity were all battery grade. (>99.5 %) The methyl propionate (MP) solvent (>99 %) was purchased from Shanghai Aladdin Co., ltd. The basic electrolyte (BE) was prepared by dissolving 1 mol/L $LiPF_6$ into the mixture of EC and DMC (1: 1 by volume). The MP-based LHCE was prepared by dissolving the LiTFSI salt into the MP and FEC mixture (9: 1 by volume) at specified molarities in the Ar-filled glovebox. For the localized high concentration electrolyte, the diluent HFE and the 5 m electrolyte was

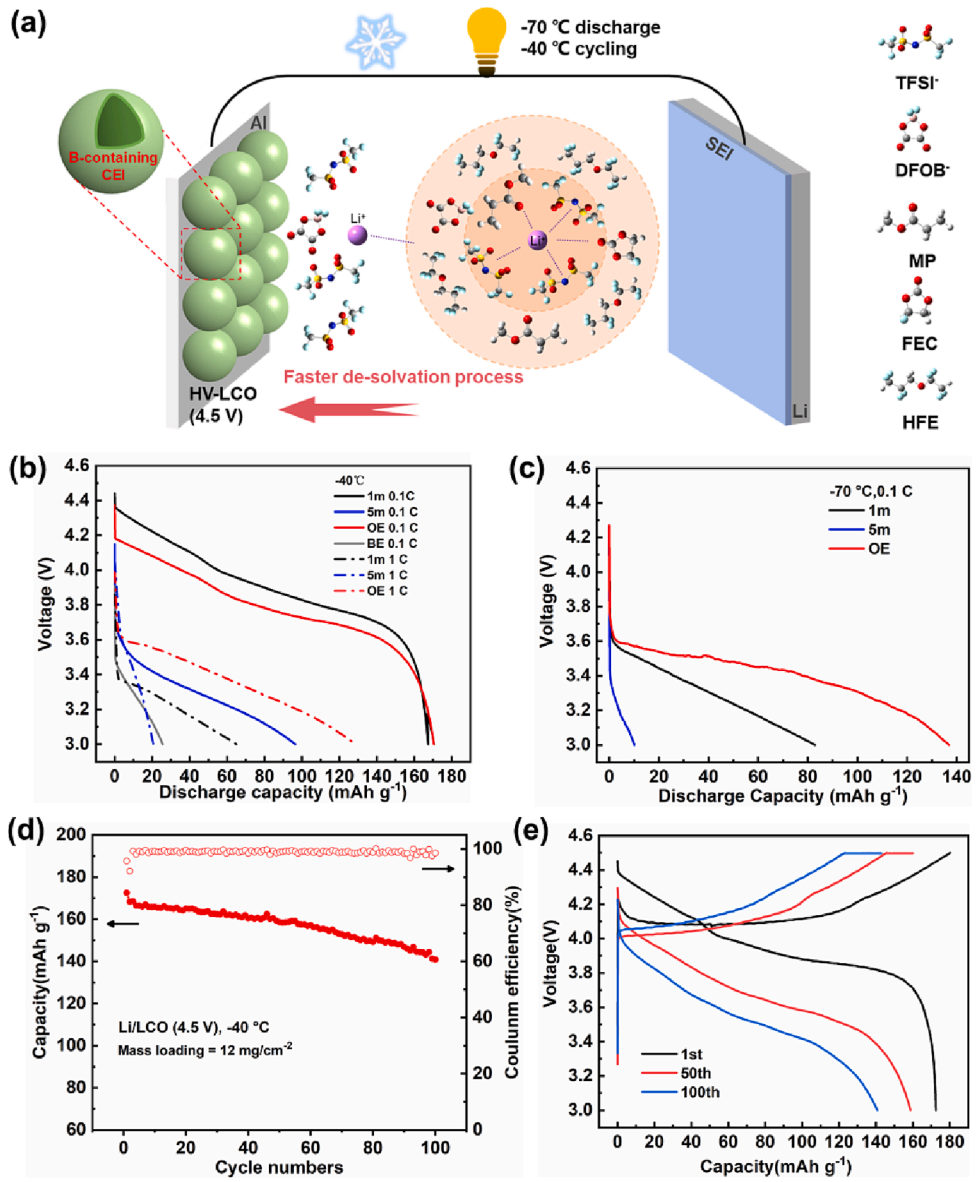

Fig. 1. (a) The scheme of the solvation structure and the interfacial chemistry at the cathode/electrolyte interface in the optimized electrolyte. (b) Discharge performance of Li/LCO cell in electrolytes at −40 °C at high rate. (c) Discharge performance of Li/LCO cell in electrolytes at −70 °C at 0.1C. (d–e) Cycling performance of Li/LCO in OE at −40 °C at 0.1C/0.5C for charge/discharge, respectively.

mixed in the specific mass ratio. For example, the 5 m-HFE21 was prepared by mixing HFE and 5 m electrolyte in the mass ratio of 2: 1. And the OE is the 5 m-HFE21 with 0.5 wt% LiDFOB. All the Li/LCO cells were assembled in 2016 type coin cell. Every Li/LCO cell was assembled by sandwiching a separator between cathode and anode and adding around 70 μL electrolyte in the glove box (M. Braun GmbH).

2.2. Computational detail

All the density functional theory (DFT) calculation was conducted on the Gaussian09 package [39]. The molecules were optimized by B3LYP-D3 method [40,41] at 6–311 + G(d,p) basis set [42,43]. The electrostatic potential (ESP) of solvent molecules was analyzed in the Multiwfn program [44,45]. The binding energy was calculated by the following equation:

$$E_{bind} = E_{total} - E_{sol} - E_{Li^+}$$

E_{total}, E_{sol} and E_{Li}^{+} represented the single point energy of lithiu complex, solvent and lithium ion respectively. As for the desolvation energy calculation, the acetone (dielectric constant 20.49) was applied as the solvent environment of the molecule in the SMD implicit solvation model [46]. The desolvation energy of solvation structure was calculated as follows:

$$E_b = E_{total} - nE_{sol} - E_{Li^+}$$

in which n is the number of solvents. E_{total}, E_{sol} and E_{Li}^{+} represented the single point energy of lithium complex, solvents and lithium ion respectively.

The classical molecular dynamics (MD) simulation was taken to investigate coordination behavior of Li^+ The MD was simulated by Gromacs 2018.8 software [47]. The force field used in this work is OPLS-AA [48]. And the force field parameters of MP, FEC HFE and LiTFSI were generated with Sobtop program. Atomic charges of Li^+ and TFSI ions were multiplied by scale factor 0.8 to correct the polarization effect [49]. The molecules were packed by Packmol software [50]. And then the packed box was submitted to energy minimization process using the steepest descent method. The equilibrium simulation was carried out with NPT ensemble at 298.2 K and 1 bar for 20 ns. The production

simulation was carried out with NVT ensemble at 298.2 K for 5 ns. The VMD software [51] was used to visualize the simulated electrolyte and get the ion association state. The anion or solvent was thought to associate with Li^+ if the distance between the atom from anion or solvent and Li^+ was less than 2.4 Å. The mean-squared displacement (MSD) of Li^+ was tracked for the last 200 ps. By analyzing the MSD result, the diffusion coefficient (D) of Li^+ in the electrolyte can be calculated by following equation:

$$D = \frac{1}{6N_a}\lim_{t\to\infty}\frac{d}{dt}\sum_{i=1}^{Na}\langle[r_i(t) - r_i(0)]^2\rangle = \frac{1}{6}\lim_{t\to\infty}\frac{d}{dx}MSD$$

in which N_a is the number of atoms. r_i *(t)* and r_i *(0)* is the position of atom i at time t and time 0.

2.3. Material characterization

The conductivity of electrolytes was characterized by using current (AC) impedance module assembled in CHI660D electrochemical workstation. The conductivity of electrolyte at different temperatures was obtained by the following equation:

$$\sigma = \frac{l}{Ra}$$

In this equation, σ is the conductivity of electrolyte, l represents the length of two platinum plane, a means the area of platinum plane, R is determined by the section point value of AC impedance. The viscosity of electrolyte was obtained by the VM-10A-L viscometer. The temperature-dependent conductivity and viscosity measurement was measured after staying at setting temperature for at least 30 min. The contact angle test was taken to evaluate the wettability of electrolyte with separator and was conducted by JC-2000C1 contact angle tester.

The X-ray diffraction (XRD) test was taken in Rigaku miniflex 600 X-ray diffractometer with Cu K2 target. The XRD test angle was ranged from 10° to 80° with the scanning speed of 5° min^{-1}. Scanning electron microscope (SEM) images were taken from Gemini SEM 500 field emission scanning electron microscope manufactured from Zeiss company. The transmission electron macroscope (TEM) images of LCO cathode were obtained from FEI Tecnai F30 instrument. X-ray photoelectron spectroscopy (XPS) results were obtained from Escalab Xi + equipment. The LCO cathode and lithium metal sample for the tests above was obtained from disassembled cell and rinsed with DMC solvent for 3 times in Ar-filled glovebox. During the transferring process, the prepared sample was protected in the well-sealed container filled with Ar gas to avoid the contact with oxygen in the air. Nuclear Magnetic Resonance (NMR) of ^7Li was tested by Ascend 500 MHz spectrometer. The NMR tube with a capillary tube containing 0.1 M $LiClO_4$ salt dissolved in D_2O solution for locking field in the ^7Li NMR tests [30]. Raman test was conducted by HORIBA FRANCE and the wavelength of the laser was 532 nm.

2.4. Electrochemical characterization

The electrochemical impedance spectroscopy (EIS) test was taken in Solartron Metrology at a frequency from 10^{-1} Hz to 10^5 Hz with a voltage amplitude of 5 mV. The linear sweep voltammetry (LSV) data was obtained in CHI660D electrochemical workstation by using a two-electrode system where the stainless steel was used as working electrode and lithium metal was used as reference and counter electrode. The sweeping speed in LSV test was set at 1 mV s^{-1} with the voltage range from 3.0 V to 5.5 V. The Tafel curve data was also obtained in CHI660D electrochemical workstation by using Li/Li symmetrical 2032 type coin cell. The testing speed was 1 mV s^{-1} in the range from −1.5 V to 1.5 V. The average Coulombic efficiency (CE) of different electrolytes was calculated using a modified Adam method 3[52]. The Li/Cu cells were firstly deposited at amount of 5 mAh cm^{-2} as a Li reservoir, and then were deposited and stripped at amount of 1 mAh cm^{-2} for ten cycles. The cell was cycled at a current density of 0.5 mA cm^{-2}. The CE was calculated by the following equation:

$$CE = \left(\frac{cyclenumber \times Q_c + Q_s}{cyclenumber \times Q_c + Q_f}\right) \times 100\%$$

where Q_f is the first deposition capacity of 5 mAh cm^{-2}, Q_c is the deposition capacity of 1 mAh cm^{-2} during the cycling and Q_s is the final charge capacity. The Li^+ transference number was estimated with the AC impedance measurements on a Li/Li symmetrical 2032-type cells and was calculated in the following equation:

$$t_{Li^+} = \frac{I_s(\Delta V - I_0R_0)}{I_0(\Delta V - I_sR_s)}$$

in which ΔV is the applied voltage of 10 mV, I_0 and I_s is the initial and steady-state current and R_0 and R_s is the corresponding impedance of the cell.

All the batteries were assembled in glove box full of Ar gas with water and oxygen content less than 0.5 ppm. The charging/discharging behavior of cell in different electrolytes was studied in the Neware test system. The potential of Li/LCO cell was ranged from 3.0 to 4.5 V. For the room temperature test, the Li/LCO cell was initially activated for one cycle at rate of 0.1C (1C = 180 mAh g^{-1}), followed by 1C rate cycling. The low temperature environment was provided by DC-8006 incubator for the discharge test and Meiling Biology & Medical DW-HW50 ultra-low freezer for the cycling test. All the tests for the cell for low temperature test were conducted after two activation cycles at 0.1C rate at room temperature. The activated cell was placed in the chamber and stayed for 2 h to reach the thermal equilibrium.

3. Results and discussion

Firstly, the low temperature performance of cell in different electrolytes was investigated in Fig. 1. The 4.5 V Li/LCO cell in OE could deliver much more capacity than any other electrolytes at −40 °C at higher rate while in the traditional carbonate electrolyte (BE), it could deliver less than 30 mAh g^{-1}capacity at 0.1C and did not work at 1C rate. It is worth noting that the addition amount of LiDFOB has an impact of the discharge performance of cells at low temperature, the OE is still best among them (Fig. S1). Apart from that, the cell in OE delivered 136.9 mAh g^{-1}capacity at −70 °C at 0.1C, demonstrating the outstanding ultra-low temperature performance (Fig. 1c). To our surprise, the high loading Li/LCO cell with OE can be cycled at −40 °C, maintaining 77.8 % after 100 cycles, suggesting the improved electrochemical kinetics at low temperature (Fig. 1d and 1e). These results show that OE is capable for the high-voltage batteries in the cryogenic condition.

The excellent electrochemical performance of cell at cryogenic condition is related to the physical properties of electrolytes. Due to the lower freeze point and better solubility of the MP solvent, the MP-based electrolyte could maintain the liquid state at lower temperature (Fig. S2), while the BE is frozen at around −30 °C and has remarkable variation in conductivity (Fig. 2a). On the other hand, the introduction of the diluent reduces the electrolyte's viscosity dramatically from 425 mPa·s of 5 m to 31.1 mPa·s of 5 m-HFE21 (Fig. 2b). The diffusion behavior of Li^+ can be calculated by tracking the mean square displacement (MSD) for the last 200 ps as displayed in the Fig. S3. The diffusion coefficient of OE is higher than that of 5 m electrolyte and surpass 1 m electrolyte at lower temperature. The values of diffusion coefficient of different electrolytes are listed in Table S1. The decent conductivity and viscosity at low temperature and the calculated MSD results indicate that OE has good ion transportation ability in the bulk electrolyte at low temperature. Also, the charge transfer process at electrode/electrolyte interface, which is regarded as the limiting factor at low temperature [53], is investigated by the electrochemical impedance spectroscopy (EIS) test (Fig. S4). According to the difference of

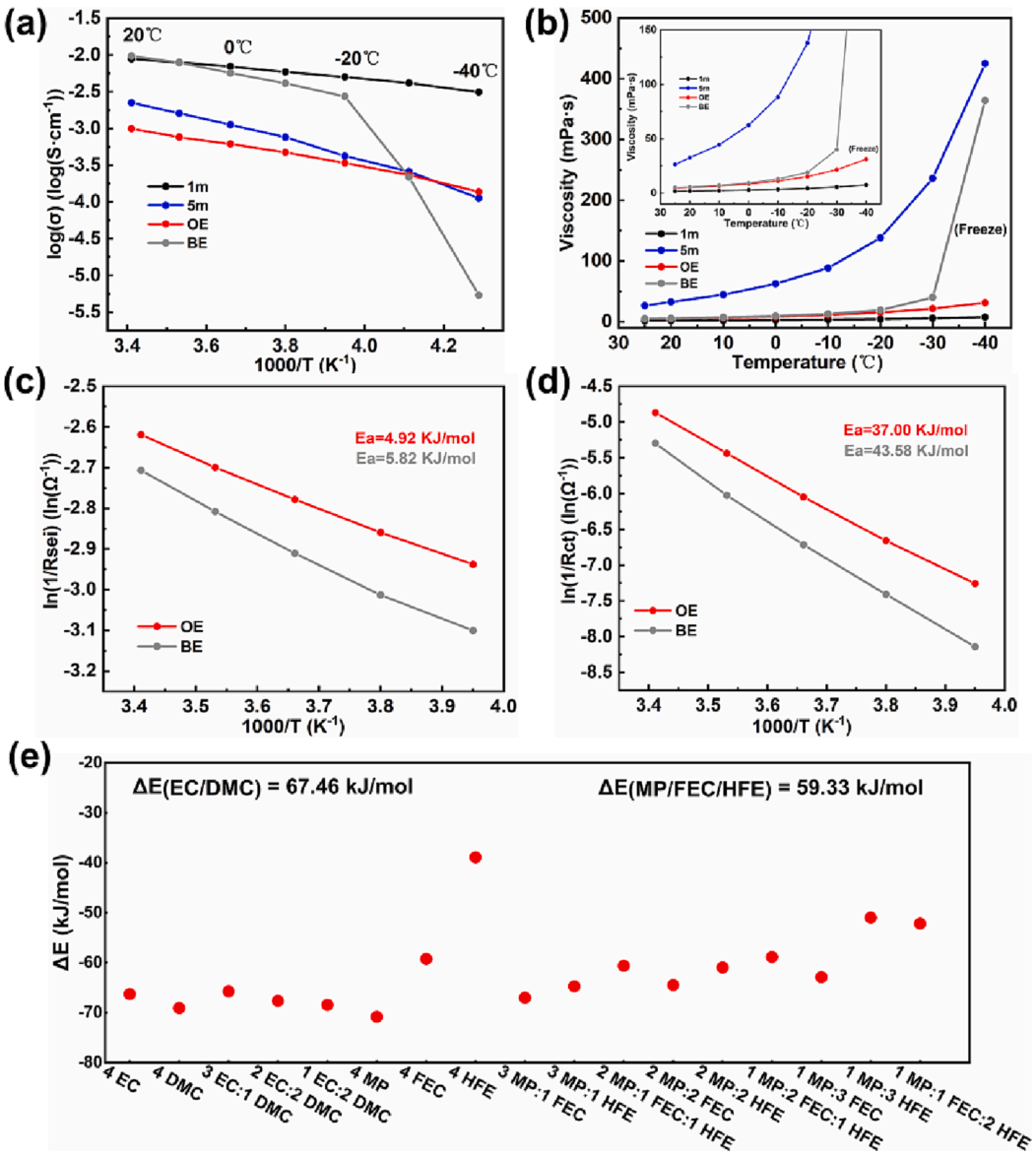

Fig. 2. The (a) conductivity and (b) viscosity of electrolytes at different temperature. (c-d) Calculated activated energy of Rct and Rsei of the two electrolytes. (e) The calculated average solvation/desolvation energy of different (solvent)$_4$-Li$^+$ clusters.

frequency, the resistance of cell can be divided into bulk resistance R_b, SEI resistance R_{sei}, charge transfer resistance R_{ct} and warburg diffusion resistance W [54]. It is obvious that the cell's total resistance especially R_{ct} increases as temperature reduces. Based on the increase of R_{ct} and R_{sei}, the calculated corresponding activation energy is displayed in Fig. 2c and d, respectively. Whatever in the diffusion across the SEI or charge transfer process, the activation energy of Li/LCO cell in OE was lower than that in BE, indicating the faster kinetic during the cycling. And also, the result of transport number indicated that although the conductivity of OE is much lower than that of BE, the higher transport number of OE enabled it has good ion transportation in the bulk electrolyte (Fig. S5). Apart from that, in the Tafel test, the exchange current density of OE is higher than that of BE, suggesting the fast Li^+ transfer kinetic at the electrode/electrolyte interface (Fig. S6). We guess the improved kinetics can be ascribed to the two aspects: (1) the reduced viscosity and improved wettability due to the addition of the diluent; (2) the unique solvation structure with low desolvation energy of the optimized electrolyte. As for the latter, it has been reported in previous literature that the anion combined with Li^+ is repulsed when approaching the negative-polarized anode and the binding energy of Li^+/anion has often been neglected in previous studies [28,55–57]. Nevertheless, the solvation/desolvation energy of possible Li^+/solvents solvation structures are calculated and listed in Fig. 2e. It can be found that MP-based electrolyte demonstrated lower average binding energy than carbonate-based electrolyte, contributing to its better low temperature performance. In addition, the OE also exhibits the excellent rate performance, delivering ≈ 75 % capacity (135.3 mAh g^{-1}) at 10C rate, which is much higher than that in carbonate electrolyte. (Fig. S7).

According to previous literature [29,56], the charge transfer process and its temperature dependence are closely related to the solvation environment of Li^+. Therefore, the MP-based electrolyte's solvation structure was investigated by theoretical calculation and experiments, the results are displayed in Fig. 3. The Raman spectra of electrolytes in Fig. 3a show that the chemical shift of LiTFSI salt [58] moves to higher wave number as the increase of salt concentration, indicating the enhancement of corporation between Li^+ and TFSI anion. Meanwhile, the introduction of diluent does not significantly alter the wave number, indicating the maintenance of the inner solvation structure. On the other hand, by the characterization of ^{7}Li NMR in Fig. 3b, it can be found that as the salt concentration increased, the chemical shift of electrolytes

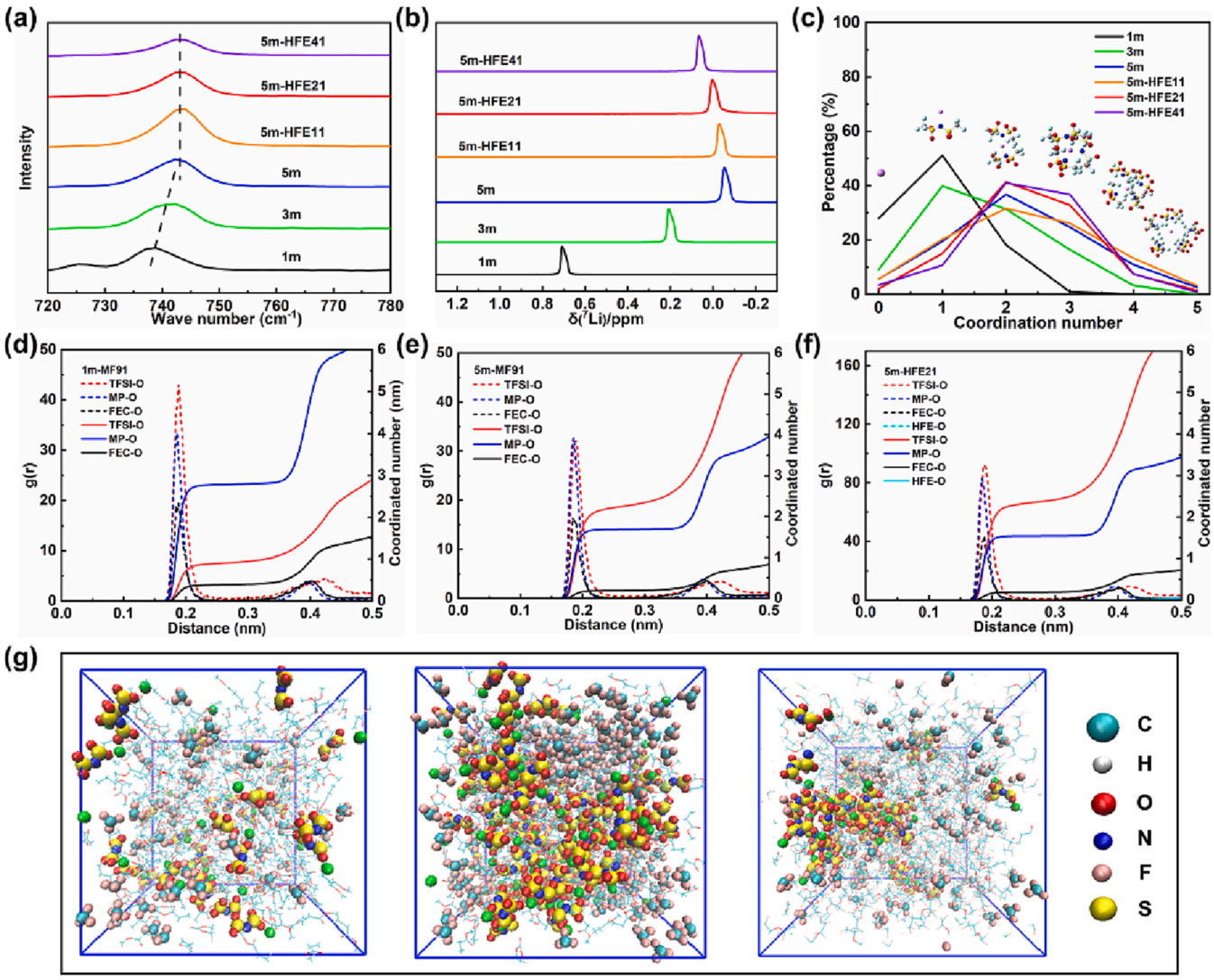

Fig. 3. (a) Raman spectra of electrolytes in the range from 720 and 780 cm^{-1}. (b) ^{7}Li NMR spectra of electrolytes. (c) Ionic association conditions of different electrolytes. (d–f) RDF and CN of three electrolytes. (g) MD snapshots of LCE (1 m), HCE (5 m) and LHCE (5 m-HFE21).

moves to the higher field.

The spectral results above are consistent with the MD simulation (Fig. 3c to 3 g). Within the first solvation sheath (the distance from lithium ion is less than 2.5 Å), the dominant structure at low concentration electrolyte (LCE) is solvent-separated ion-pair (SSIP), in which Li^+ coordinates with solvent molecules. While in the HCE or LHCE, more lithium ions are coordinated with salt anion, forming contact-ion-pair (CIP) or aggregate (AGG) [59]. The detailed association state of Li^+ with other components is listed in Table S2-S5. The coordination number (CN) and radial distribution functions (RDF, g(r)) of other electrolytes were shown in Fig. S8. The CN of Li^+ is listed in Table S6. It can be observed that the CN of Li^+ with O in MP solvent is decreased from 2.8 in LCE to 1.7 in HCE and the CN of Li^+ with O in anion is increased from 0.9 to 2.2, indicating more anions enter the inner solvation structure. While in the LHCE, the CN of Li^+ is nearly the same with HCE, suggesting the inner solvation structure did not significantly altered after the addition of diluent. As previous literature demonstrated, the CIP/AGG dominated system is advantageous in the low temperature environment [56]. Therefore, by comprehensive comparison, LHCE is an ideal electrolyte in terms of ion desolvation process or ion transportation in the bulk electrolyte due to its high proportion of CIP/AGG and low transportation resistance. Also, it is worth noting that benefited from the anion-containing solvation structure and reduced solvent molecules, the HCE and LHCE demonstrate the wider voltage window compared with the LCE (Fig. S9).

The cycling performance of high-voltage Li/LCO cell at room temperature at 1C rate is shown in Fig. 4a and 4b. In 1 m electrolyte, the cell was overcharged at 65th cycle, which is probably resulted from the decomposition of electrolyte at 4.5 V. While in the 5 m electrolyte, albeit it shows the superior cycling performance, the relatively poor electrode/electrolyte interface is still detrimental to the cycling stability. To further improve it, moderate amount of diluent and LiDFOB additive were added into the HCE. On the one hand, the introduction of diluent improved the wettability between electrolyte and separator (Fig. S10) and did not change the inner Li^+ solvation structure due to its weak solvating ability with Li^+ (Fig. S11). On the other hand, after adding small amount of LiDFOB additive, the solvation structure of lithium ion was altered, which has a great impact on the decomposition behavior of electrolyte (this will be further discussed in the Fig. S12). When the DFOB-solvated Li^+ approached the surface of cathode, the DFOB anion decomposed prior to other components and formed B-containing cathode/electrolyte interface (CEI) as the DFT calculation and LSV results revealed (Fig. S13 and S14). Therefore, addition of LiDFOB additive can prevent the further side reaction of cathode at high voltage, which will be discussed later. By comparing the electrochemical performance of the batteries in different amount of diluent and additive, the OE shown the

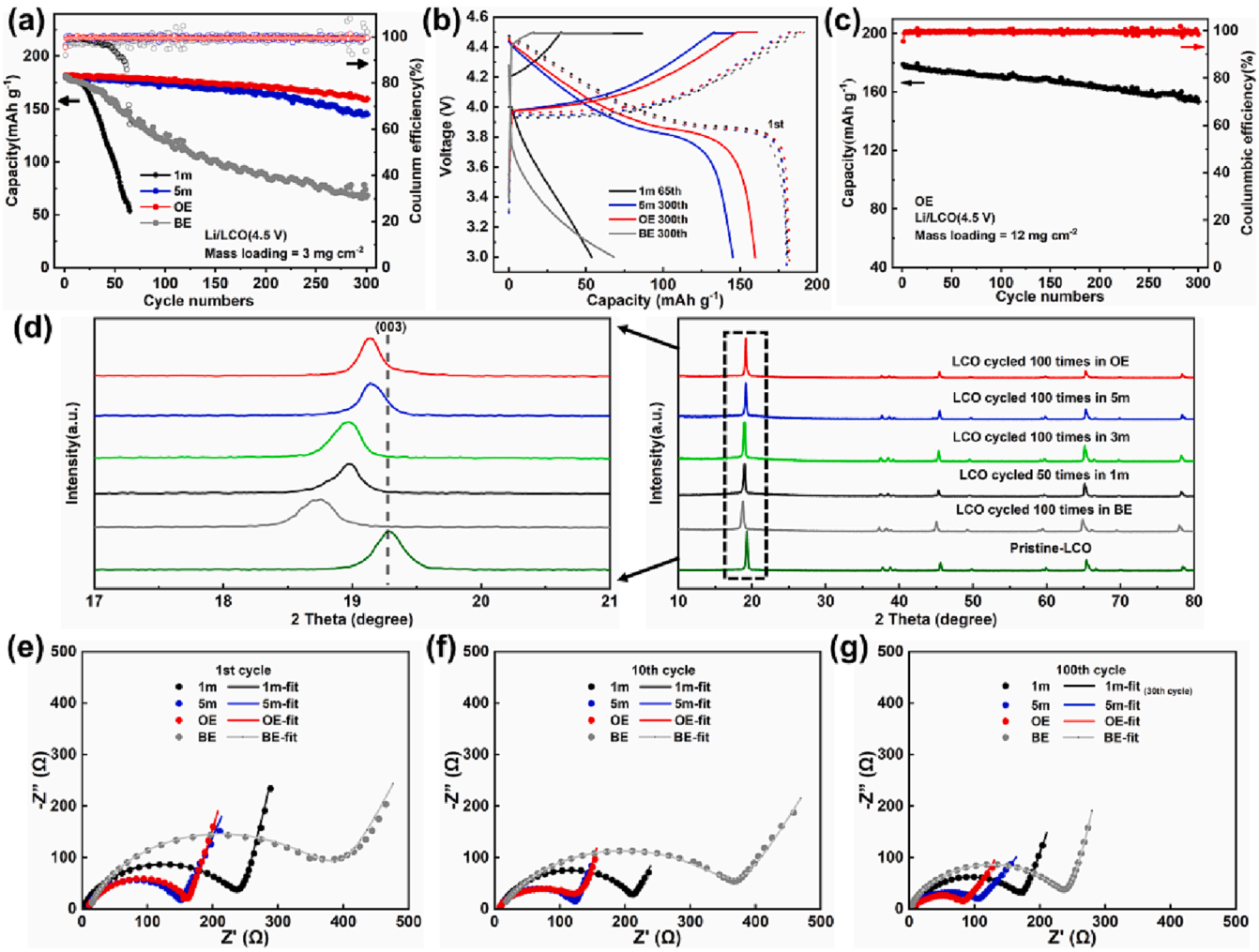

Fig. 4. (a) Electrochemical performance of Li/LCO cell in four electrolytes at 1C rate. (b) Voltage-specific capacity curves of the electrolytes. (c) Electrochemical performance of the high-mass-loading Li/LCO cell in OE at 0.3C / 0.5C for charge / discharge, respectively. (d) XRD result of LCO material in Li/LCO cell with different electrolytes. (e-g) EIS result of Li/LCO cell in the four electrolytes for (e) 1cycle, (f) 10 cycles and (g) 100 cycles.

best cycling performance among them (Fig. S15). With the OE, the Li/LCO cell remained 87.7 % capacity retention after 300 cycles at 1C rate. As a comparison, the BE only delivered 37.6 % capacity retention after 300 cycles due to the oxidation of electrolyte at 4.3 V. Also, it is worth mentioning that with the high loading Li/LCO cell with OE remained 85.2 % capacity after 300 cycles at 0.3C / 0.5C for charge / discharge, respectively (Fig. 4c).

The stable cycling performance of cell is proved by the XRD characterization result. As shown in Fig. 4d, the (0 0 3) peak of LCO in different electrolyte exhibits different degree of movement compared with pristine sample [60]. And (0 0 3) peak of LCO cathode with BE and 1 m electrolyte exhibited a greater amplitude after cycling, suggesting more serious irreversible phase transition which is related to electrochemical performance of battery. However, there is a small variation in the 5 m and OE, suggesting their degree of irreversibility are not so serious. The similar trend can also be found in another characteristic (1 0 4) peak at around 45° (Fig. S16). Also, such a different degree of irreversibility corresponds to different SEM images of LCO cathode cycled in electrolytes before and after 200 cycles (Fig. S17). Additionally, the interfacial impedance value of Li/LCO cell in different electrolytes at different cycles are demonstrated in Fig. 4e to 4 g and it can be observed that the cell in 1 m and BE electrolyte have higher impedance value. By the comparisons above, the characterization results are all consistent with the battery's electrochemical performance.

The electrochemical performance of batteries is closely related to the electrolyte/electrode interface, which is affected by the component of electrolyte. To explore it, the TEM and XPS characterization on the cathode were conducted. The results are displayed in Fig. 5. From the morphology of LCO cathode cycled after 20 cycles in the four electrolytes, it can be observed that the CEI layer generated in 1 m electrolyte is quite thick, which is not favorable for the long-term cycling. Also, as the C 1 s and O 1 s spectra of XPS result shown, the surface of cathode in 1 m electrolyte is mainly composed of lithium carbonate (Li_2CO_3, 288.6 eV, C 1 s) and alkoxy lithium (LiOR, 531.2 eV, O 1 s), which were probably generated from the decomposition of free solvent molecule in 1 m electrolyte and were not capable to protect cathode at high voltage. Besides, the observed M−O signal indicated that there may be the leakage of transition metal ion from electrode to electrolyte during cycling [23]. As for the 5 m electrolyte, the thickness of CEI is relatively thin and its chemical component is mostly derived from the decomposition of salt anion (e.g. LiF). And the electrochemical window of 5 m electrolyte could inhibit the aluminum corrosion resulted from the LiTFSI (Fig. S18). For the 5 m-HFE21 electrolyte without LiDFOB, the proportion of LiF and organic component is increased, which perhaps ascribed to the decomposition of the HFE diluent (Fig. S19) [61]. After adding diluent and additive together, the CEI becomes quite thin and uniform. In addition, the organic component of the cathode surface decreased obviously, suggesting the inhibited deposition of electrolyte. From F 1 s and O 1 s spectra, it can be found the introduction of LiDFOB leads to the B-containing components in the CEI (B-F, 685.2 eV, F 1 s and

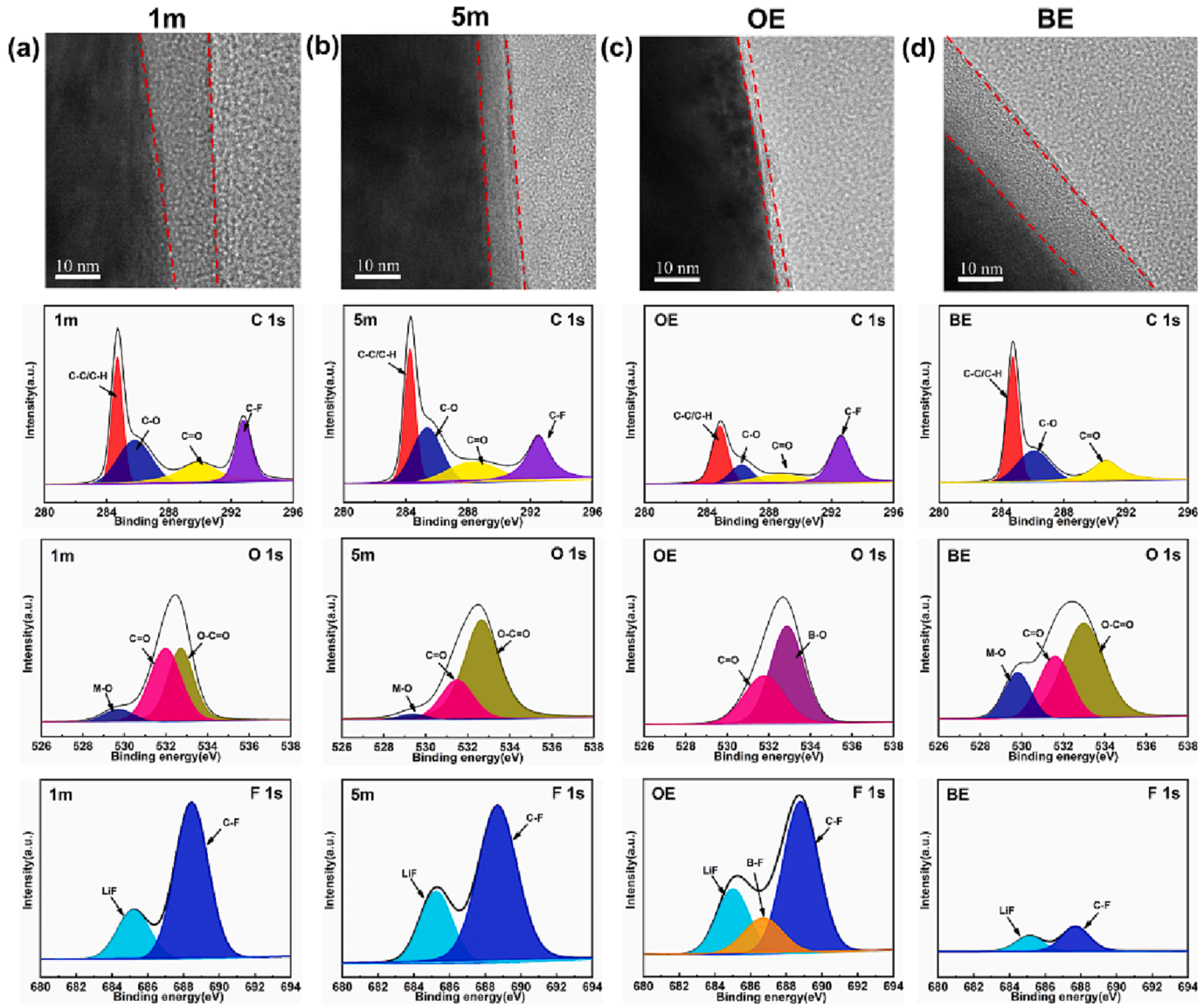

Fig. 5. TEM images and XPS results of LCO cathode in the four electrolytes after 20 cycles. (a) 1 m (b) 5 m (c) OE (d) BE.

B-O, 532.8 eV, O 1 s), which is regarded beneficial for protecting the cathode [62,63]. And these results are corresponded to the B 1 s spectra (Fig. S20). As for the BE electrolyte, it also suffers from severe decomposition as 1 m electrolyte do, and has much thicker CEI layer. (Fig. 5d) Apart from cathode, the Coulombic efficiency Li/Cu cell was tested and the cell with OE could reach 98.6 %, higher than those with other electrolytes (Fig. S21). Also, the morphology of cycled lithium metal anode in OE indicates that it has better compatibility with lithium metal anode. (Fig. S22) These results above show that our optimized electrolyte is stable with cathode and anode, which corresponds to cell's electrochemical stability.

4. Conclusion

In conclusion, we report a designed MP-based LHCE with LiDFOB additive and confirm its solvation structure by experiments and theoretical calculations. This LHCE combines both advantages of low viscosity of LCE and anion-dominated solvation structure of HCE, showing the superiority in high-voltage cycling and low temperature application. Besides, the addition of LiDFOB alters the solvation structure and assists to form B-containing CEI, which further improves the cycling performance of cell. As a result, the optimized electrolyte enables 4.5 V Li/LCO cell to remain 87.7 % capacity for 300 cycles at 1C rate. Also, it delivers around 75 % capacity at 10C high-rate, demonstrating the superior rate performance. As for the low temperature performance, this electrolyte demonstrates a high discharge capacity retention of 76.0 % at −70 °C and shows an excellent charge/discharge behavior at −40 °C. All in all, this work provides a designing method for an electrolyte with the multifunction of high voltage, fast dynamic and low temperature.

Declaration of Competing Interest

The authors declare that they have no known competing financial interests or personal relationships that could have appeared to influence the work reported in this paper.

Data availability

The authors do not have permission to share data.

Acknowledgement

We gratefully acknowledge the financial support of National Key Research and Development Program of China (2021YFB2400300),

National Natural Science Foundation of China (21875198,21875195), the Fundamental Research Funds for the Central Universities (20720190040) and the key Project of Science and Technology of Xiamen (3502Z20201013). And we are grateful to Tan Kah Kee Innovation Laboratory (IKKEM) for help with XPS, SEM, NMR and Raman measurements. In terms of DFT calculation and MD simulation, we were appreciative to Beijng PARATERA Tech CO., Ltd. for HPC resources (URL: https://paratera.com/).

Appendix A. Supplementary data

Supplementary data to this article can be found online at https://doi.org/10.1016/j.cej.2023.141904.

References

[1] B. Scrosati, J. Hassoun, Y.-K. Sun, Lithium-ion, batteries., A look into the future, Energy Environ. Sci. 4 (9) (2011), https://doi.org/10.1039/c1ee01388b.
[2] J.-M. Tarascon, M. Armand, Issues and challenges facing rechargeable lithium batteries, Nature 414 (2001) 359–367, https://doi.org/10.1038/35104644.
[3] R.V. Noorden, The rechargeable revolution- a better battery, Nature 507 (2014) 26–28, https://doi.org/10.1038/507026a.
[4] X. Zeng, M. Li, D. Abd El-Hady, W. Alshitari, A.S. Al-Bogami, J. Lu, K. Amine, Commercialization of lithium battery technologies for electric vehicles, Adv. Energy Mater. 9 (27) (2019) 1900161.
[5] M. Armand, J.-M. Tarascon, Building better batteries, Nature 451 (7) (2008) 652–657, https://doi.org/10.1038/451652a.
[6] J. Fan, On the discharge capability and its limiting factors of commercial 18650 Li-ion cell at low temperatures, J. Power Source 117 (1–2) (2003) 170–178, https://doi.org/10.1016/s0378-7753(03)00354-9.
[7] N. Zhang, T. Deng, S. Zhang, C. Wang, L. Chen, C. Wang, X. Fan, Critical review on low-temperature Li-ion/metal batteries, Adv. Mater. 34 (15) (2022), https://doi.org/10.1002/adma.202107899.
[8] J. Zhang, J. Zhang, T. Liu, H. Wu, S. Tian, L. Zhou, B. Zhang, G. Cui, Toward low-temperature lithium batteries: advances and prospects of unconventional electrolytes, Adv. Energy Sustain. Res. 2 (10) (2021) 2100039.
[9] G.U. Yue-ru, Z.H.A.O. Wei-min, S.U. Chang-hu, L.U.O. Chuan-jun, Z.H.A.N. G. Zhong-ru, X.U.E. Xu-jin, Y. Yong, Research progresses in improvement for low temperature performance of lithium-ion batteries, J. Electroanal. Chem. 24 (5) (2018) 488–496, https://doi.org/10.13208/j.electrochem.180145.
[10] W. Xue, T. Qin, Q. Li, M. Zan, X. Yu, H. Li, Exploiting the synergistic effects of multiple components with a uniform design method for developing low-temperature electrolytes, Energy Stor. Mater. 50 (2022) 598–605, https://doi.org/10.1016/j.ensm.2022.06.003.
[11] L. Dong, Y. Liu, K. Wen, D. Chen, D. Rao, J. Liu, B. Yuan, Y. Dong, Z. Wu, Y. Liang, M. Yang, J. Ma, C. Yang, C. Xia, B. Xia, J. Han, G. Wang, Z. Guo, W. He, High-polarity fluoroalkyl ether electrolyte enables solvation-free Li(+) transfer for high-rate lithium metal batteries, Adv. Sci. (Weinh) 9 (5) (2022) e2104699.
[12] A.C. Thenuwara, P.P. Shetty, M.T. McDowell, Distinct nanoscale interphases and morphology of lithium metal electrodes operating at low temperatures, Nano Lett. 19 (12) (2019) 8664–8672, https://doi.org/10.1021/acs.nanolett.9b03330.
[13] N. Gao, Y. Zhang, C. Chen, B. Li, W. Li, H. Lu, L. Yu, S. Zheng, B. Wang, Low-temperature Li–S battery enabled by CoFe bimetallic catalysts, J. Mater. Chem. A 10 (15) (2022) 8378–8389, https://doi.org/10.1039/d2ta00406b.
[14] Z.K. Liu, J. Guan, H.X. Yang, P.X. Sun, N.W. Li, L. Yu, Ternary-salt solid polymer electrolyte for high-rate and long-life lithium metal batteries, Chem. Commun. (Camb) 58 (78) (2022) 10973–10976, https://doi.org/10.1039/d2cc04128f.
[15] L. Wang, B. Chen, J. Ma, G. Cui, L. Chen, Reviving lithium cobalt oxide-based lithium secondary batteries-toward a higher energy density, Chem. Soc. Rev. 47 (17) (2018) 6505–6602, https://doi.org/10.1039/c8cs00322j.
[16] M. Li, C. Wang, Z. Chen, K. Xu, J. Lu, New concepts in electrolytes, Chem. Rev. 120 (14) (2020) 6783–6819, https://doi.org/10.1021/acs.chemrev.9b00531.
[17] X. Zheng, L. Huang, X. Ye, J. Zhang, F. Min, W. Luo, Y. Huang, Critical effects of electrolyte recipes for Li and Na metal batteries, Chem 7 (9) (2021) 2312–2346, https://doi.org/10.1016/j.chempr.2021.02.025.
[18] H. Wang, Z. Yu, X. Kong, S.C. Kim, D.T. Boyle, J. Qin, Z. Bao, Y.i. Cui, Liquid electrolyte: the nexus of practical lithium metal batteries, Joule 6 (3) (2022) 588–616.
[19] J. Hou, M. Yang, D. Wang, J. Zhang, Fundamentals and challenges of lithium ion batteries at temperatures between −40 and 60 °C, Adv. Energy Mater. 10 (18) (2020) 1904152.
[20] Y. Yan, S. Weng, A. Fu, H. Zhang, J. Chen, Q. Zheng, B. Zhang, S. Zhou, H. Yan, C.-W. Wang, Y. Tang, H. Luo, B.-W. Mao, J. Zheng, X. Wang, Y.u. Qiao, Y. Yang, S.-G. Sun, Tailoring electrolyte dehydrogenation with trace additives: stabilizing the $LiCoO_2$ cathode beyond 4.6 V, ACS Energy Lett. 7 (8) (2022) 2677–2684.
[21] Z. Sun, H. Zhou, X. Luo, Y. Che, W. Li, M. Xu, Design of a novel electrolyte additive for high voltage LiCoO2 cathode lithium-ion batteries: lithium 4-benzonitrile trimethyl borate, J. Power Source 503 (2021) 230033.
[22] X.u. Liu, X. Sun, X. Shi, D. Song, H. Zhang, C. Li, K.-Y. Wang, C. Xiao, X. Liu, L. Zhang, Low-temperature and high-performance Si/graphite composite anodes enabled by sulfite additive, Chem. Eng. J. 421 (2021) 127782.
[23] S. Lin, J. Zhao, Functional electrolyte of fluorinated ether and ester for stabilizing both 4.5 V LiCoO2 cathode and lithium metal anode, ACS Appl. Mater. Interfaces 12 (7) (2020) 8316–8323, https://doi.org/10.1021/acsami.9b21679.
[24] T. Fan, W. Kai, V.K. Harika, C. Liu, A. Nimkar, J.G. Nicole Leifer, S. Maiti, M. N. Tsubery, X. Liu, M. Wang, X.u. Leimin, L.u. Yuhao, Y. Min, D. Netanel Shpigel, Aurbach,, Operating highly stable LiCoO2 cathodes up to 4.6 V by using an effective integration of surface engineering and electrolyte solutions selection, Adv. Funct. Mater. (2022), https://doi.org/10.1002/adfm.202204972.
[25] Q. Liu, H. Xu, F. Wu, D. Mu, L. Shi, L. Wang, J. Bi, B. Wu, Effects of a high-concentration LiPF6-based carbonate ester electrolyte for the electrochemical performance of a high-voltage layered LiNi0.6Co0.2Mn0.2O2 cathode, ACS Appl. Energy Mater. 2 (12) (2019) 8878–8884, https://doi.org/10.1021/acsaem.9b01917.
[26] J. Li, H. Hua, X. Deng, P. Lai, Y. Kang, S. Kuang, F. Wang, X. Zeng, Y. Zhang, J. Zhao, Mild and controllable solid electrolyte interphase formation for high-voltage lithium metal batteries in a wide-temperature range from −40 °C to 80 °C, Chem. Eng. J. 452 (2023) 139398.
[27] Y. Yamada, J. Wang, S. Ko, E. Watanabe, A. Yamada, Advances and issues in developing salt-concentrated battery electrolytes, Nat. Energy 4 (4) (2019) 269–280, https://doi.org/10.1038/s41560-019-0336-z.
[28] T. Feng, G. Yang, S. Zhang, Z. Xu, H. Zhou, M. Wu, Low-temperature and high-voltage lithium-ion battery enabled by localized high-concentration carboxylate electrolytes, Chem. Eng. J. 433 (2022) 134138.
[29] J. Holoubek, K. Kim, Y. Yin, Z. Wu, H. Liu, M. Li, A. Chen, H. Gao, G. Cai, T. A. Pascal, P. Liu, Z. Chen, Electrolyte design implications of ion-pairing in low-temperature Li metal batteries, Energy Environ. Sci. 15 (4) (2022) 1647–1658, https://doi.org/10.1039/d1ee03422g.
[30] S. Lin, H. Hua, P. Lai, J. Zhao, A multifunctional dual-salt localized high-concentration electrolyte for fast dynamic high-voltage lithium battery in wide temperature range, Adv. Energy Mater. 11 (36) (2021) 2101775.
[31] M.C. Smart, B.V. Ratnakumar, K.B. Chin, L.D. Whitcanack, Lithium-ion electrolytes containing ester cosolvents for improved low temperature performance, J. Electrochem. Soc. 157 (12) (2010) A1361.
[32] A. Ohta, H. Koshina, H. Okuno, H. Murai, Relationship between carbonaceous materials and electrolyte in secondary lithium-ion batteries, J. Power Source 54 (1) (1995) 6–10.
[33] R. Petibon, J. Harlow, D.B. Le, J.R. Dahn, The use of ethyl acetate and methyl propanoate in combination with vinylene carbonate as ethylene carbonate-free solvent blends for electrolytes in Li-ion batteries, Electrochim. Acta 154 (2015) 227–234, https://doi.org/10.1016/j.electacta.2014.12.084.
[34] J.-P. Jones, M.C. Smart, F.C. Krause, R.V. Bugga, The effect of electrolyte additives upon lithium plating during low temperature charging of graphite-LiNiCoAlO2 lithium-ion three electrode cells, J. Electrochem. Soc 167 (2) (2020) 020536.
[35] P. Lai, H. Hua, B. Huang, P. Zhang, J. Zhao, A carboxylic ester-based electrolyte with additive to improve performance of lithium batteries at ultra-low temperature, J. Electrochem. Soc. 169 (10) (2022) 100539.
[36] G. Cai, J. Holoubek, D. Xia, M. Li, Y. Yin, X. Xing, P. Liu, Z. Chen, An ester electrolyte for lithium-sulfur batteries capable of ultra-low temperature cycling, Chem. Commun. (Camb.) 56 (64) (2020) 9114–9117, https://doi.org/10.1039/d0cc03798b.
[37] B.o. Liao, H. Li, M. Xu, L. Xing, Y. Liao, X. Ren, W. Fan, L.e. Yu, K. Xu, W. Li, Designing low impedance interface films simultaneously on anode and cathode for high energy batteries, Adv. Energy Mater. 8 (22) (2018) 1800802.
[38] J. Cha, J.-G. Han, J. Hwang, J. Cho, N.-S. Choi, Mechanisms for electrochemical performance enhancement by the salt-type electrolyte additive, lithium difluoro (oxalato)borate, in high-voltage lithium-ion batteries, J. Power Source 357 (2017) 97–106, https://doi.org/10.1016/j.jpowsour.2017.04.094.
[39] M.J. Frisch, G.W. Trucks, D.J. Fox, Gaussian 09, Revision E. 01, Gaussian, Inc., Wallingford CT, (2013).
[40] S. Grimme, J. Antony, S. Ehrlich, H. Krieg, A consistent and accurate ab initio parametrization of density functional dispersion correction (DFT-D) for the 94 elements H-Pu, J. Chem. Phys. 132 (15) (2010), 154104, https://doi.org/10.1063/1.3382344.
[41] P.J. Stephens, F.J. Devlin, C.F. Chabalowski, M.J. Frisch, Ab initio calculation of vibrational absorption and circular dichroism spectra using density functional force fields, J. Phys. Chem. 98 (45) (1994) 11623–11627.
[42] R. Krishnan, J.S. Binkley, R. Seeger, J.A. Pople, Self-consistent molecular orbital methods. XX. A basis set for correlated wave functions, J. Chem. Phys. 72 (1) (1980) 650–654.
[43] T. Clark, J. Chandrasekhar, G.W. Spitznagel, P.V.R. Schleyer, Efficient diffuse function-augmented basis sets for anion calculations. III. The 3-21+G basis set for first-row elements, Li-F, J. Comput. Chem. 4 (3) (1983) 294–301.
[44] T. Lu, F. Chen, Multiwfn: a multifunctional wavefunction analyzer, J. Comput. Chem. 33 (5) (2012) 580–592, https://doi.org/10.1002/jcc.22885.
[45] J. Zhang, T. Lu, Efficient evaluation of electrostatic potential with computerized optimized code, Phys. Chem. Chem. Phys. 23 (36) (2021) 20323–20328, https://doi.org/10.1039/d1cp02805g.
[46] A.V. Marenich, C.J. Cramer, D.G. Truhlar, Universal solvation model based on solute electron density and on a continuum model of the solvent defined by the bulk dielectric constant and atomic surface tensions, J. Phys. Chem. B 113 (18) (2009) 6378–6396.
[47] M.J. Abraham, T. Murtola, R. Schulz, S. Páll, J.C. Smith, B. Hess, E. Lindahl, GROMACS: high performance molecular simulations through multi-level parallelism from laptops to supercomputers, SoftwareX 1–2 (2015) 19–25, https://doi.org/10.1016/j.softx.2015.06.001.

[48] William L. Jorgensen, David S. Maxwell, Julian Tirado-Rives, Development and Testing of the OPLS All-Atom Force Field on Conformational Energetics and Properties of Organic Liquids, Journal of the American Chemical Society 118(45) (1996) 11225-11236. https://doi.org/10.1021/ja9621760.
[49] C. Park, M. Kanduč, R. Chudoba, A. Ronneburg, S. Risse, M. Ballauff, J. Dzubiella, Molecular simulations of electrolyte structure and dynamics in lithium–sulfur battery solvents, J. Power Source 373 (2018) 70–78, https://doi.org/10.1016/j.jpowsour.2017.10.081.
[50] L. Martinez, R. Andrade, E.G. Birgin, J.M. Martinez, PACKMOL: a package for building initial configurations for molecular dynamics simulations, J. Comput. Chem. 30 (13) (2009) 2157–2164, https://doi.org/10.1002/jcc.21224.
[51] W. Humphrey, A. Dalke, K. Schulten, Andrew Dalke, K Schulten, VMD: visual molecular dynamics, J. Mol. Graph. 14 (1) (1996) 33–38.
[52] B.D. Adams, J. Zheng, X. Ren, W.u. Xu, J.-G. Zhang, Accurate determination of coulombic efficiency for lithium metal anodes and lithium metal batteries, Adv. Energy Mater. 8 (7) (2018) 1702097.
[53] Q. Li, D. Lu, J. Zheng, S. Jiao, L. Luo, C.M. Wang, K. Xu, J.G. Zhang, W. Xu, Li+-Desolvation dictating lithium-ion battery's low-temperature performances, ACS Appl. Mater. Interfaces 9 (49) (2017) 42761–42768, https://doi.org/10.1021/acsami.7b13887.
[54] S.S. Zhang, K. Xu, T.R. Jow, Electrochemical impedance study on the low temperature of Li-ion batteries, Electrochim. Acta 49 (7) (2004) 1057–1061, https://doi.org/10.1016/j.electacta.2003.10.016.
[55] P. Bai, J. Li, F.R. Brushett, M.Z. Bazant, Transition of lithium growth mechanisms in liquid electrolytes, Energy Environ. Sci. 9 (10) (2016) 3221–3229, https://doi.org/10.1039/c6ee01674j.
[56] J. Holoubek, H. Liu, Z. Wu, Y. Yin, X. Xing, G. Cai, S. Yu, H. Zhou, T.A. Pascal, Z. Chen, P. Liu, Tailoring electrolyte solvation for Li metal batteries cycled at ultra-low temperature, Nat. Energy 6 (3) (2021) 303–313.
[57] C. Wang, B. Nan, L. Chen, N.D. Rodrigo, O. Borodin, N. Piao, J. Xia, T. Pollard, S. Hou, J. Zhang, X. Ji, J. Xu, X. Zhang, L. Ma, X. He, S. Liu, H. Wan, E. Hu, W. Zhang, K. Xu, X.Q. Yang, B. Lucht, Enhancing Li+ transport in NMC811, graphite lithium-ion batteries at low temperatures by using low-polarity-solvent electrolytes, Angew. Chem. Int. Ed. Engl. (2022), https://doi.org/10.1002/anie.202205967.
[58] B.K. Mandal, A.K. Padhi, Z. Shi, S. Chakraborty, R. Filler, LiTFSI New low temperature electrolytes with thermal runaway inhibition for lithium-ion rechargeable batteries, J. Power Source 162 (1) (2006) 690–695.
[59] Y. Yamada, K. Furukawa, K. Sodeyama, K. Kikuchi, M. Yaegashi, Y. Tateyama, A. Yamada, Unusual stability of acetonitrile-based superconcentrated electrolytes for fast-charging lithium-ion batteries, J. Am. Chem. Soc. 136 (13) (2014) 5039–5046, https://doi.org/10.1021/ja412807w.
[60] L. Wang, J. Ma, C. Wang, X. Yu, R. Liu, F. Jiang, X. Sun, A. Du, X. Zhou, G. Cui, A novel bifunctional self-stabilized strategy enabling 4.6 V LiCoO2 with excellent long-term cyclability and high-rate capability, Adv. Sci. (Weinh) 6 (12) (2019) 1900355, https://doi.org/10.1002/advs.201900355.
[61] X. Ren, L. Zou, X. Cao, M.H. Engelhard, W. Liu, S.D. Burton, H. Lee, C. Niu, B. E. Matthews, Z. Zhu, C. Wang, B.W. Arey, J. Xiao, J. Liu, J.-G. Zhang, W. Xu, Enabling high-voltage lithium-metal batteries under practical conditions, Joule 3 (7) (2019) 1662–1676, https://doi.org/10.1016/j.joule.2019.05.006.
[62] S. Jiao, X. Ren, R. Cao, M.H. Engelhard, Y. Liu, D. Hu, D. Mei, J. Zheng, W. Zhao, Q. Li, N. Liu, B.D. Adams, C. Ma, J. Liu, J.-G. Zhang, W. Xu, Stable cycling of high-voltage lithium metal batteries in ether electrolytes, Nat. Energy 3 (9) (2018) 739–746, https://doi.org/10.1038/s41560-018-0199-8.
[63] M. Hu, J. Wei, L. Xing, Z. Zhou, Effect of lithium difluoro(oxalate)borate (LiDFOB) additive on the performance of high-voltage lithium-ion batteries, J. Appl. Electrochem. 42 (5) (2012) 291–296, https://doi.org/10.1007/s10800-012-0398-0.